

Cross-species analysis traces adaptation of Rubisco toward optimality in a low-dimensional landscape

Yonatan Savir^a, Elad Noor^b, Ron Milo^b, and Tsvi Tlusty^{a,1}

^aDepartment of Physics of Complex Systems and ^bDepartment of Plant Sciences, Weizmann Institute of Science, Rehovot 76100, Israel

Edited by George H. Lorimer, University of Maryland, College Park, MD, and approved December 17, 2009 (received for review October 8, 2009)

Rubisco (D-ribulose 1,5-bisphosphate carboxylase/oxygenase), probably the most abundant protein in the biosphere, performs an essential part in the process of carbon fixation through photosynthesis, thus facilitating life on earth. Despite the significant effect that Rubisco has on the fitness of plants and other photosynthetic organisms, this enzyme is known to have a low catalytic rate and a tendency to confuse its substrate, carbon dioxide, with oxygen. This apparent inefficiency is puzzling and raises questions regarding the roles of evolution versus biochemical constraints in shaping Rubisco. Here we examine these questions by analyzing the measured kinetic parameters of Rubisco from various organisms living in various environments. The analysis presented here suggests that the evolution of Rubisco is confined to an effectively one-dimensional landscape, which is manifested in simple power law correlations between its kinetic parameters. Within this one-dimensional landscape, which may represent biochemical and structural constraints, Rubisco appears to be tuned to the intracellular environment in which it resides such that the net photosynthesis rate is nearly optimal. Our analysis indicates that the specificity of Rubisco is not the main determinant of its efficiency but rather the trade-off between the carboxylation velocity and CO₂ affinity. As a result, the presence of oxygen has only a moderate effect on the optimal performance of Rubisco, which is determined mostly by the local CO₂ concentration. Rubisco appears as an experimentally testable example for the evolution of proteins subject both to strong selection pressure and to biochemical constraints that strongly confine the evolutionary plasticity to a low-dimensional landscape.

enzyme specificity | photosynthesis | protein evolution | carbon fixation

Photosynthetic carbon assimilation enables the storage of energy in the global ecosystem and produces most of the global biomass. Rubisco (D-ribulose 1,5-bisphosphate carboxylase/oxygenase), probably the most abundant enzyme in nature (1), catalyzes the addition of CO₂ and H₂O (2, 3) to 1,5-ribulose biphosphate (RuBP) in the first major step of carbon fixation through photosynthesis. Rubisco is present in most autotrophic organisms from prokaryotes, such as photosynthetic anaerobic bacteria and cyanobacteria, to eukaryotes, such as algae and higher plants (4). The catalytic rate of Rubisco is remarkably slow. On top of that, Rubisco tends to catalyze the addition of O₂ instead of CO₂, leading to photorespiration that entails an extra energy investment and a reduction in the net photosynthetic rate (5). The seeming contradiction between the importance of Rubisco and its apparent inefficiency motivated an ongoing effort to improve Rubisco by genetic manipulation (6) and directed evolution (7, 8), with very limited success so far. One would desire to increase the specificity of Rubisco to CO₂ and its rate of carboxylation. However, this task proves difficult because the specificity and the carboxylation velocity appear to be negatively correlated (9). A possible biochemical mechanism for this trade-off was recently proposed (10), following the hypothesis that Rubisco optimizes this trade-off according to its environment. The present work quantitatively addresses the questions regarding the optimality and inefficiency of Rubisco, which we suggest result from an interplay between constraints and evolutionary forces. Our analysis delineates a low-dimensional landscape shaped by underlying physico-chemical constraints in

which Rubisco evolves. Comparison of cross-species data implies that Rubisco is nearly optimal in this constrained landscape.

Carbon fixation by Rubisco is a multistage process (Fig. 1A) (11, 12). In the first stage, Rubisco binds RuBP and the formed complex undergoes enolization. This is followed by an irreversible CO₂ addition (carboxylation) that results in a six-carbon intermediate. Then, steps of hydration and cleavage yield two molecules of a three-carbon compound, 3-phosphoglycerate, which are later used to make larger carbohydrates. In the competing reaction of oxygenation, the Rubisco–RuBP complex irreversibly captures O₂ and through similar steps of hydration and cleavage yields only one 3-phosphoglycerate molecule and one molecule of 2-phosphoglycolate. To retrieve the carbons in 2-phosphoglycolate a complicated process of photorespiration takes place, incurring a net loss of CO₂ (about one CO₂ molecule per two captured O₂ molecules) (5) and thus reduces the photosynthetic carboxylation rate.

The Rubisco-catalyzed carboxylation and oxygenation are known to exhibit *effective* Michaelis–Menten (MM) kinetics (Fig. 1B) (13). The MM parameters for carboxylation are the maximal carboxylation velocity v_C , which combines the steps of hydration and cleavage, and the MM constant for CO₂ addition, K_C , which represents the effective affinity of the carbon dioxide molecule to the enolized Rubisco–RuBP complex. The carboxylation rate per Rubisco molecule, R_C , when RuBP is in saturation, takes the familiar MM form, $R_C = v_C / (1 + K_C / [\text{CO}_2] + (K_C / K_O) ([\text{O}_2] / [\text{CO}_2]))$. Addition of oxygen sequesters a fraction of the available Rubisco–RuBP complexes and is represented by the factor $[\text{O}_2] / K_O$ in the denominator, where K_O is the effective MM constant for oxygen binding. A similar expression is derived for the rate of oxygenation per Rubisco molecule, R_O (Fig. 1B). The specificity of Rubisco, S , is the ratio of the normalized carboxylation and oxygenation rates, $S = (R_C / R_O) \cdot ([\text{O}_2] / [\text{CO}_2]) = (v_C / K_C) / (v_O / K_O) = k_{\text{on},C} / k_{\text{on},O}$, which depends solely on the ratio of the addition rates. The CO₂ and O₂ concentrations that affect the kinetic parameters are not determined solely by the ambient habitat conditions. Many species developed CO₂ concentrating mechanisms (CCM) that enable the accumulation of CO₂ at the carboxylation site (14–16).

It has been suggested that the oxygenation, which leads to the low specificity of Rubisco, is an inherent side effect of biochemical constraints on the reaction (2, 3, 17, 18). However, the specificity S and other kinetic parameters do vary among species (9), which implies that selection pressure may play a role in shaping Rubisco in response to environmental changes. Correlations among the kinetic parameters from various organisms, in particular, the negative S versus v_C correlation (9, 19, 20), provide evidence for an interplay between constraints and selection and support an underlying structural mechanism (10). For example, Rubisco that has adapted to low CO₂/O₂ ratios tends to have high specificity but, on the other hand, low v_C .

Author contributions: Y.S., E.N., R.M., and T.T. performed research and wrote the paper.

The authors declare no conflict of interest.

This article is a PNAS Direct Submission.

¹To whom correspondence should be addressed. E-mail: tsvi.tlusty@weizmann.ac.il.

This article contains supporting information online at www.pnas.org/cgi/content/full/0911663107/DCSupplemental.

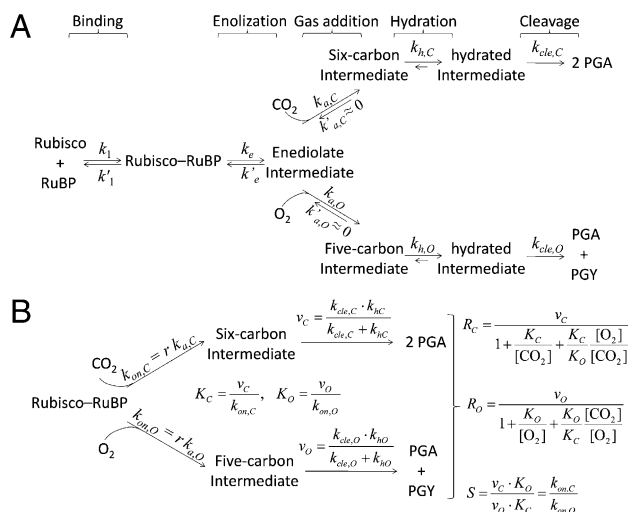


Fig. 1. Carboxylation/oxygenation by Rubisco. (A) Rubisco catalyzes the addition of CO₂ or O₂ to D-ribulose 1,5 biphosphate (RuBP). Rubisco binds RuBP to form a complex that undergoes enolization. In the case of carboxylation (Upper pathway), this is followed by practically irreversible CO₂ addition that results in a six-carbon intermediate. Through steps of hydration and cleavage, the reaction produces two molecules of 3-phosphoglycerate (3-PGA). Oxygenation follows similar steps (Lower pathway), through a five-carbon intermediate, and results in one 3-PGA and one 2-phosphoglycolate (2-PGY) (12). (B) The Rubisco-catalyzed carboxylation and oxygenation exhibit effective Michaelis–Menten (MM) kinetics. The carboxylation rate per Rubisco molecule, R_C , and oxygenation rate per Rubisco molecule, R_O , when RuBP is in saturation, take the familiar MM form (see equations in the figure). The effective kinetics consist of two irreversible steps. The effective gas binding ($k_{on,C}$ and $k_{on,O}$), which consists of the enolization of the Rubisco–RuBP complex, whose fraction is $r = k_e/(k'_e + k_e)$, and gas addition, determined by the rates $k_{a,C}$ and $k_{a,O}$. This is followed by effective catalysis (v_C and v_O), which includes the steps of hydration and cleavage. The MM constants for gas addition, K_C and K_O , are the effective affinities of the CO₂ and O₂ molecules to the Rubisco–RuBP complex (Methods).

Results

Kinetic Parameters of Rubisco Are Confined to an Effectively 1D Landscape. In the following, we examine the interplay between the biochemical constraints and the evolutionary selection pressure to optimize Rubisco by analyzing the correlations among the measured in vitro kinetic parameters (v_C , K_C , S , K_O) from various organisms. Fig. 2A presents the kinetic parameters of 28 Rubiscos collected from 27 species (Table S1), both eukaryotes and prokaryotes, which are divided into six groups: photosynthetic bacteria, cyanobacteria, green and nongreen algae, and C₃ and C₄ higher plants. A few forms of Rubisco are known: Form I (L₈S₈) is composed of eight large and eight small subunits whereas form II consists of only large subunits (4). The Rubisco we had information for and analyzed here are all of the more abundant form I except for the form II Rubisco of *Rhodospirillum rubrum* and *Rhodospseudomonas sphaeroides*.

Each species in the data set corresponds to a point in a four-dimensional space whose coordinates are the four kinetic parameters v_C , K_C , S , and K_O . When the data points are plotted in logarithmic scale (Fig. 2B), they appear to follow a straight line, which indicates that the data reside in an effectively one-dimensional space. To quantify this observation of reduced dimensionality, we performed principal component analysis (PCA) of the data (Methods). The PCA amounts to rotating the coordinate system such that as much as possible of the variability in the data lies along one axis called the first principal component, which is actually the straight line that best represents the data in terms of least squares.

We analyze the data in terms of the four parameters that determine the rates of carboxylation and oxygenation, that is, v_C ,

K_C , the ratio K_C/K_O , and S . Surprisingly, we find that the first principal component captures $\sim 91\%$ of the variability in the data (Methods) and therefore the data are indeed effectively one-dimensional. The data exhibit strong power law correlations (Fig. 2) (two significant digits are shown),

$$\begin{aligned} K_C &\propto v_C^{2.0 \pm 0.2} \\ \frac{K_C}{K_O} &\propto v_C^{1.5 \pm 0.2} \\ S &\propto v_C^{-0.51 \pm 0.1} \end{aligned} \quad [1]$$

There are two evident outliers, the only form II Rubisco of *R. rubrum* and *R. sphaeroides*, which were therefore excluded from the fit. We also tested the possibility of separate power law correlations for prokaryotes and eukaryotes (Fig. S1). However, the analysis shows that the form I prokaryotes follow almost the same trends as form I eukaryotes, thus suggesting that the more relevant division is into form I and form II Rubisco that are subject to different constraints. The dependence of K_C , S , and K_O/K_C solely on v_C signifies the effective one-dimensionality of the data. The extracted power laws manifest inherent trade-offs between the kinetic parameters of Rubisco. For example, the specificity S decreases like the square root of the carboxylation velocity v_C .

Carboxylation and Oxygenation Energetic Trade-Offs. The effective MM kinetics can be represented in terms of a free energy profile (Fig. 3A) and the power law correlations between the kinetic parameters can be translated into energetic trade-offs. The effective kinetics consist of two irreversible steps, effective gas binding (i.e., enolization and gas addition) and effective catalysis (i.e., hydrolysis and cleavage) (Fig. 1B), which correspond to two effective energy barriers. The values of the first energy barrier, $\Delta G_{1,C}$ for carboxylation and $\Delta G_{1,O}$ for oxygenation, are related to the effective gas binding rates, $k_{on,C} \sim \exp(-\Delta G_{1,C})$, $k_{on,O} \sim \exp(-\Delta G_{1,O})$. The second energy barriers, $\Delta G_{2,C}$ and $\Delta G_{2,O}$, are linked to the effective catalysis rates, $v_C \sim \exp(-\Delta G_{2,C})$, $v_O \sim \exp(-\Delta G_{2,O})$. The specificity S is simply the exponent of the difference in the energy barrier for CO₂ and O₂ addition, $S \sim \exp(\Delta G_{1,O} - \Delta G_{1,C})$.

From the phenomenological power law relations (Eq. 1) we deduce the interplay between changes in the energy barriers across species. We find two basic trade-offs: The first trade-off follows from the power law $v_C/K_C = k_{on,C} \sim 1/v_C$ (Fig. 3B). This quantitatively manifests a previously suggested trade-off between the addition of CO₂ to the enolized RuBP and the catalysis rate of this complex (10). This inverse relation can be expressed, by taking the logarithm, as the “conservation” of the sum of the carboxylation energy barriers, $\Delta G_{1,C} + \Delta G_{2,C} \approx \text{const.}$ (Fig. 3B). One may speculate that the origin of this trade-off is the partition of a certain approximately constant deformation energy, which is required for the completion of the carboxylation process, into two sequential steps. A second trade-off is between the CO₂ and O₂ addition rates, $k_{on,O} \sim k_{on,C}^{0.5}$, which indicates that a decrease in the CO₂ addition barrier is associated with a smaller decrease, by a factor of $\frac{1}{2}$, in the O₂ addition barrier (Fig. 3C) such that $0.5 \cdot \Delta G_{1,C} - \Delta G_{2,O} \approx \text{const.}$ These two basic trade-offs can be combined into the apparent trade-off between specificity and carboxylation velocity, $S = k_{on,C}/k_{on,O} \sim v_C^{-0.5}$. An increase in the specificity is not due to a lower O₂ binding rate, $k_{on,O}$, which actually increases, but due to an even faster increase of the CO₂ binding rate, $k_{on,C}$. This increase resembles the recently suggested conformational proofreading mechanism (21, 22) in which conformational changes—in the case of Rubisco, possibly linked to the closure of loop 6 (23)—simultaneously vary the rates of two competing reactions such that the overall specificity increases. No significant correlation is observed between the effective O₂ catalysis rate v_O and the rest of the parameters (Fig. S2). This observation hints that this reaction stage is only weakly coupled to the main trade-offs and thus v_O values can be selected

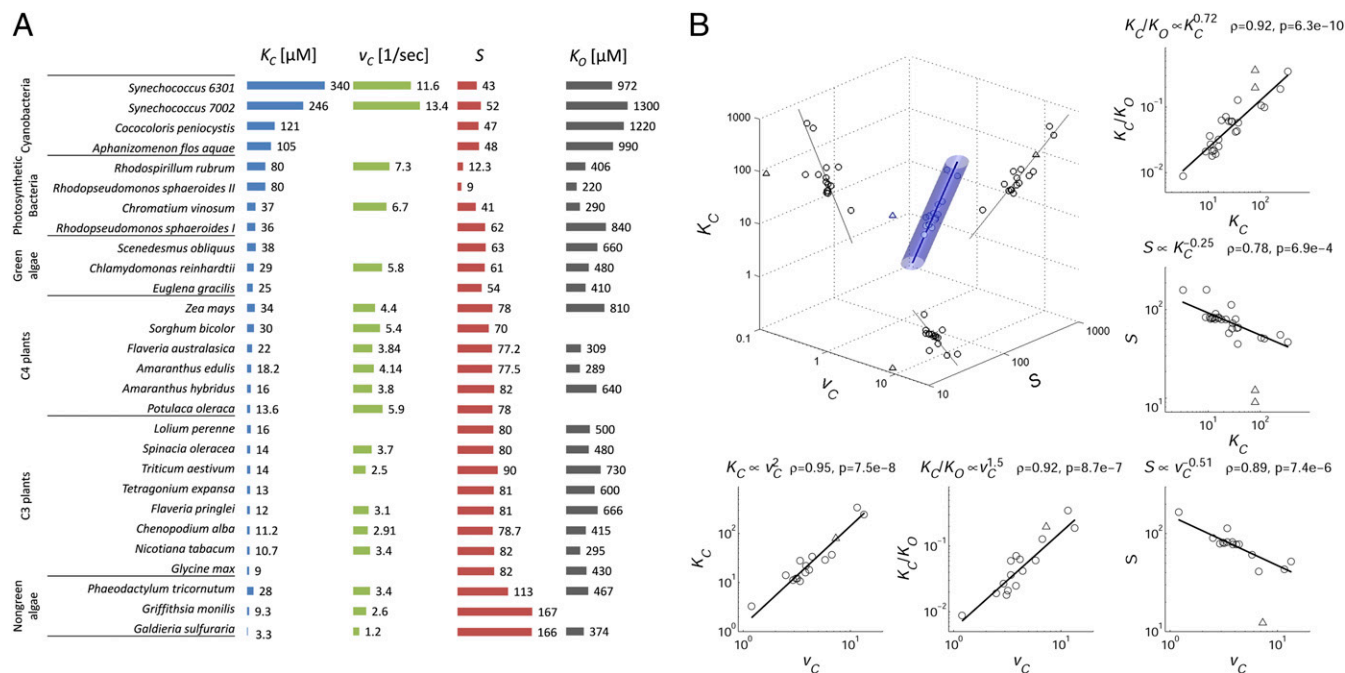


Fig. 2. Power law correlations among kinetic parameters of Rubisco define the 1D landscape. (A) The four kinetic parameters of 28 Rubiscos from 27 species (Table S1): the effective Michaelis–Menten (MM) constant for CO₂ binding, K_C [μM]; the maximal carboxylation rate, v_C [1/s]; the specificity, S ; and the effective MM constant for O₂ binding, K_O [μM]. The parameters K_C and S are known for all 28 Rubiscos. For 25 Rubiscos K_O is known and for 16 Rubiscos all of the kinetic parameters are available. All Rubiscos in the dataset are of the more abundant form I besides the form II Rubiscos from *R. rubrum* and *R. sphaeroides*. (B) (Top Left) A 3D projection of the 4D kinetic parameter data. Data from the 16 species for which all four kinetic parameters are available are graphed in logarithmic scale. Each of the 16 species is represented by a point whose coordinates are its v_C , K_C , and S (blue circles). The plot depicts the PCA result that the data are confined to an effectively 1D space and follow, in logarithmic scale, a straight line (blue cylinder). The cylinder axis is the first principal axis and its radius is the standard deviation from this axis. There is one evident outlier (blue triangle), the Rubisco from *R. rubrum*, the only form II Rubisco in this set. (Top Right and Bottom) Total least-squares fit of the data from all 28 Rubiscos (Methods) to a 1D power law model (black lines). The fits are plotted in logarithmic scale and exhibit clear power law correlations between the kinetic parameters. The correlation coefficient, ρ , and the P value, p , are shown. As before, there are clear outliers (black triangles) that correspond to the form II species, *R. rubrum* and *R. sphaeroides*. Note that deviations of form II species from the model are significant mostly in its projections onto the specificity parameter S .

for independently. Another possibility is that due to the relatively low O₂ concentrations, which are rarely above K_O (Fig. 2A), the strongly selected quantity is $k_{on,O} = v_O/K_O$ and not v_O itself.

Adaptation of Rubisco in the 1D Landscape Is Nearly Optimal. A longstanding question is the level of adaptation of Rubisco to its environment. The correlations between the kinetic parameters suggest the existence of underlying biochemical and structural limitations that constrain the evolution of Rubisco. The power law relations between the kinetic parameters of Rubisco depict an effectively one-dimensional landscape that allows us to quantitatively examine the optimality of Rubisco under these “design constraints.” As a measure of the fitness of Rubisco we use the net photosynthesis rate (NPR) per Rubisco molecule, f , which is the difference between the fixed CO₂ and the CO₂ lost due to oxygenation (24). For each fixed mole of O₂ molecule $t \approx \frac{1}{2}$ mol of CO₂ are lost and the NPR is therefore $f = R_C - t \cdot R_O$. The NPR depends on the four parameters, v_C , K_C , S , and K_C/K_O . However, these parameters are not independent and thus the NPR is a 1D landscape determined by one kinetic parameter, for example v_C ,

$$f = \frac{v_C - 3 \cdot 10^{-3} \cdot ([O_2]/[CO_2]) \cdot v_C^{3/2}}{1 + 1.3 \cdot v_C^2/[CO_2] + 5 \cdot 10^{-3} \cdot ([O_2]/[CO_2]) \cdot v_C^{3/2}}, \quad [2]$$

where the concentrations are given in micromoles and v_C in units of 1/s. The NPR in a given intracellular environment exhibits a clear maximum as a function of v_C . For example, Rubisco of C₃ plants, which lack a CCM, operate at [CO₂] of ~ 7 – $8 \mu\text{M}$, whereas

Rubisco of C₄ plants, which have a CCM, experience CO₂ concentrations that are at least 10 times larger (25). Comparison of the optimal v_C to the measured ones (Fig. 4A) indicates that the Rubisco from C₄ plants is nearly optimal at [CO₂] = 80 μM whereas C₃ plants are too slow for this environment.

In the absence of oxygen ([O₂] = 0) the NPR is simply the carboxylation rate, $f = R_C = v_C/(1 + K_C/[CO_2]) = v_C/(1 + 1.3 \cdot v_C^2/[CO_2])$. The evident optimum is the direct outcome of the trade-off between the CO₂ affinity and the carboxylation velocity, $K_C \sim v_C^2$. At the limit of low v_C , K_C is also low ($K_C \ll [CO_2]$) and the enzyme is in saturation. Thus, f increases linearly with v_C , $f \sim v_C$. At the other extreme of high v_C and K_C ($K_C \gg [CO_2]$) the NPR decreases due to the fact that the affinity increases faster than the velocity and thus, $f \sim 1/v_C$. We find simple expressions for the optimal values of the kinetic parameters that bring f to its optimum f^* in an anaerobic environment:

$$\begin{aligned} v_C^* &\cong 0.86 \cdot [CO_2]^{1/2} \\ K_C^* &\cong [CO_2] \\ S^* &\cong 164 \cdot [CO_2]^{-1/4} \end{aligned} \quad [3]$$

The resulting optimal NPR is about half of the maximal carboxylation velocity, $f^* \sim v_C^*/2 \sim 0.43 \cdot [CO_2]^{1/2} \text{ s}^{-1}$. The coefficient of the specificity power law of ~ 160 indicates a difference between the gas addition barriers of ~ 3 – $5 k_B T$ that coincides with previous estimations (23).

In aerobic environments, the presence of oxygen reduces the net photosynthesis in two ways (Fig. 4A and B), sequestering a fraction

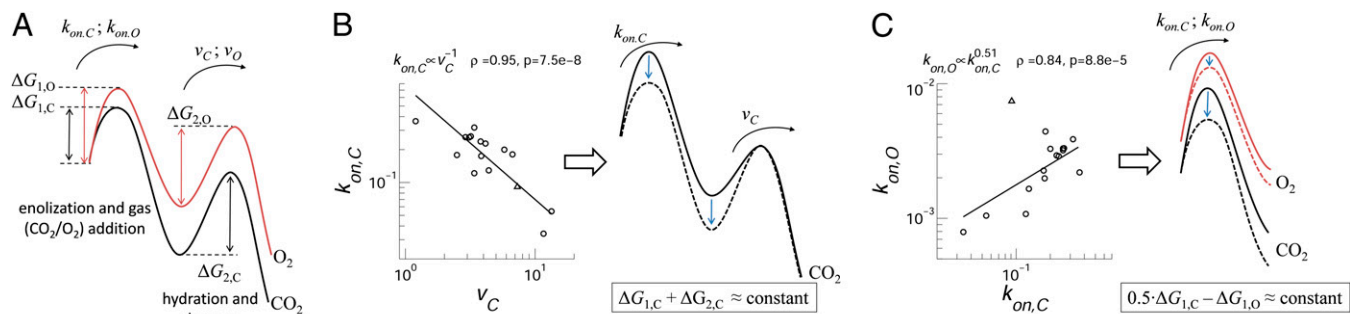


Fig. 3. The free energy trade-offs. (A) Representation of the effective Michaelis–Menten (MM) kinetics in terms of free energy profiles. The effective kinetics consist of two irreversible steps, effective gas binding (i.e., enolization and gas addition) and effective catalysis (i.e., hydrolysis and cleavage) (Fig. 1B), which correspond to two effective energy barriers. The first energy barriers are related to the rates of effective gaseous addition, $k_{on,C} \sim \exp(-\Delta G_{1,C})$, $k_{on,O} \sim \exp(-\Delta G_{1,O})$. The second barriers are linked to the effective catalysis rates, $v_C \sim \exp(-\Delta G_{2,C})$, $v_O \sim \exp(-\Delta G_{2,O})$. The specificity depends on the difference between the first energy barriers, $S = \exp(\Delta G_{1,O} - \Delta G_{1,C})$. (B) The power law correlation $k_{on,C} \propto v_C^{-1}$ ($\rho = 0.95$, $p = 7.5e-8$) (solid line, triangle is the *R. rubrum* outlier), indicates that a shift in carboxylation barrier, $\Delta G_{2,C}$, is accompanied by a shift by the same magnitude in the CO₂ addition barrier, such that their sum is conserved, $\Delta G_{1,C} + \Delta G_{2,C} = \text{const}$. The change in $\Delta G_{2,C}$ involves only a shift in the intermediate energy level but may also involve a shift in the catalysis transition-state level. (C) Another trade-off arises from the correlation between the effective addition rates of CO₂ and O₂, $k_{on,O} = v_O/K_O \sim (v_C/K_C)^{0.5} = k_{on,C}^{0.5}$ (solid line, triangle is the *R. rubrum* outlier). This indicates that a decrease in the CO₂ addition barrier, $\Delta G_{1,C}$, is associated with a smaller (by a factor of $\frac{1}{2}$) decrease in the O₂ addition barrier, $\Delta G_{1,O}$, such that $0.5 \cdot \Delta G_{1,C} - \Delta G_{2,O} = \text{const}$. The negative correlation between v_C and S is the outcome of the two trade-offs: As v_C decreases, $k_{on,C}$ increases and, as a result, $k_{on,O}$ also increases, but by a smaller factor, and the difference between the gas addition barriers increases resulting in a decrease of the specificity, $S = \exp(\Delta G_{1,O} - \Delta G_{1,C})$.

of the available Rubisco, akin to competitive inhibition, and the loss of CO₂ due to O₂ fixation, which subtracts from f a factor of $t \cdot R_O$. Because of these two effects, the presence of oxygen shifts the optimal carboxylation velocity v_C^* to lower values, overall improving the specificity and reducing oxygen addition. For example, for [CO₂] = 80 μ M, oxygen levels of 260 μ M lead to a reduction of $\sim 17\%$ in NPR and 7% in v_C^* due to Rubisco sequestering, whereas another 3% reduction in NPR and 1% in v_C^* is due to O₂ fixation (Fig. 4A). It is evident that the optimal value of the carboxylation velocity v_C^* is dictated by the concentration of

CO₂ and both effects of oxygen are only smaller corrections. Approximate expressions that include the effect of oxygen on the optimal kinetic parameters are

$$\begin{aligned} v_C^* &= 0.86 \cdot [\text{CO}_2]^{1/2} (1 - \delta_O) \\ K_C^* &= [\text{CO}_2] (1 - 2 \cdot \delta_O) \\ S_C^* &= 164 \cdot [\text{CO}_2]^{-1/4} (1 + 0.5 \cdot \delta_O). \end{aligned} \quad [4]$$

The small parameter $\delta_O = 10^{-3} \cdot [\text{O}_2][\text{CO}_2]^{-1/4}$ accounts for the effect of oxygen, which for all relevant conditions ranges between

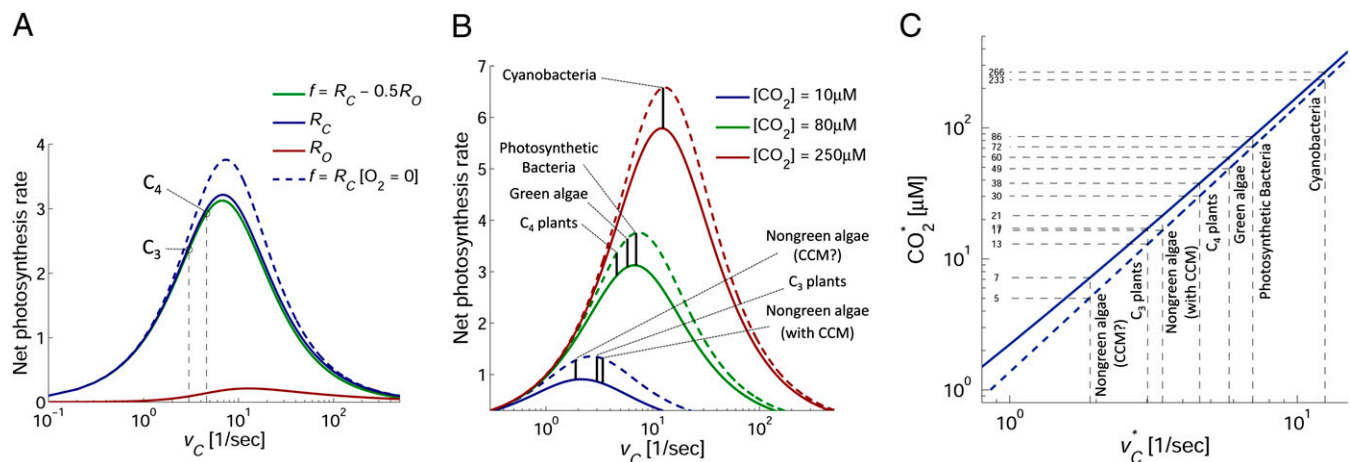


Fig. 4. The optimality of Rubisco. (A) Carboxylation rate, R_C , oxygenation rate, R_O , and net photosynthesis rate, $f = R_C - 0.5 \cdot R_O$, as a function of carboxylation velocity, v_C , for [CO₂] = 80 μ M. In an anaerobic environment the NPR equals the carboxylation rate, $f = R_C$ ([O₂] = 0) (blue dashed line) and exhibits a clear optimum. The presence of oxygen, [O₂] = 260 μ M, reduces the NPR (green line) in two ways: R_C (blue line) is reduced because oxygenation sequesters a fraction of the available Rubisco, an effect that is responsible for most of the NPR decrease. A smaller reduction of the NPR is due to the photorespiration factor, $0.5 \cdot R_O$ (red line). The presence of oxygen shifts the optimal carboxylation velocity v_C^* toward lower values (4). Most of the shift in v_C^* is due to the decrease in R_C rather than the increase in R_O . For example, C₃ plants that operate at [CO₂] \approx 7–8 μ M are far from the optimal values for [CO₂] = 80 μ M. However, C₄ plants possess CCM and operate at CO₂ concentrations that are at least 10 times larger than those of C₃ plants and their carboxylation rates are nearly optimal at [CO₂] = 80 μ M. (B) The NPR as a function of v_C for three environments, [CO₂] = 10, 80, and 250 μ M, which correspond to groups with no CCM (C₃ plants and some algae), medium-range CCM (C₄ plants, some algae, and photosynthetic bacteria), and strong CCM (cyanobacteria). The average v_C of each class is plotted and appears to be close to the values that yield maximal NPR. The solid and dashed curves correspond to aerobic and anaerobic conditions, [O₂] = 260 and 0 μ M, respectively. The optimal parameters of Rubisco are determined mostly by the CO₂ concentration. (C) The CO₂ environments that are predicted to be optimal to the observed v_C from Eq. 4 (dashed line, anaerobic; solid line, [O₂] = 260 μ M). Cyanobacteria are optimal in the CO₂-rich environment, [CO₂]^{*} \approx 240 μ M. C₄ plants, algae, and photosynthetic bacteria are optimal at intermediate CO₂ levels, [CO₂]^{*} \approx 30–80 μ M. C₃ plants and nongreen algae, which are suspected to lack CCM, are optimal at low CO₂ levels, [CO₂]^{*} \approx 5–15 μ M.

0 and 15%. In other words, the specificity of Rubisco is not the main determinant of its efficiency but rather the v_C - K_C trade-off between the carboxylation velocity and affinity is the dominant effect. The resulting optimal NPR is reduced by the presence of oxygen as $f^* = 0.45 \cdot [\text{CO}_2]^{1/2} (1 - 2 \cdot \delta_O)$ and the reduction ranges between 0 and 30%.

To further examine the optimality of Rubisco, we have to consider the intracellular environments of various organisms that are characterized by the concentrations of carbon dioxide and oxygen at the carboxylation site. Many species have the capacity to increase the local concentration of CO_2 above the passive concentration by CCM. Therefore, besides the environment of $\text{CO}_2 = 80 \mu\text{M}$ discussed above, which corresponds to medium-range CCM (some C_4 plants, some algae, and anaerobic bacteria) (15, 16, 25–28), we also plot the net photosynthesis rate for two other typical carbon dioxide concentrations (Fig. 4B): $[\text{CO}_2] = 10 \mu\text{M}$, which corresponds to the groups of no CCM (C_3 plants and some algae) (14–16, 28), and $[\text{CO}_2] = 250 \mu\text{M}$, which corresponds to strong CCM (cyanobacteria) (15, 16, 28, 29). As there is only limited knowledge of the accurate values of $[\text{CO}_2]$ and $[\text{O}_2]$ for each species, the values we use are merely gross estimates that represent coarse classification into three typical environments.

For all classes of species, we find that the observed carboxylation velocity and CO_2 effective binding affinity are close to the optimal values, v_C^* and K_C^* . This is also demonstrated in Fig. 4C, which shows the optimal environment, $[\text{CO}_2]^*$, that corresponds to a measured carboxylation velocity. We find that the cyanobacteria are optimal in a CO_2 -rich environment, $[\text{CO}_2]^* \approx 240 \mu\text{M}$, whereas C_4 plants, algae, and photosynthetic bacteria are optimal in intermediate CO_2 levels, $[\text{CO}_2]^* \approx 30$ – $80 \mu\text{M}$. Finally, C_3 plants and nongreen algae that are believed to lack CCM are optimal at CO_2 levels of 5–15 μM . As a measure for the performance of Rubisco, it is instructive to look at a landscape of the normalized NPR (Fig. 5A), where a value of unity means that the Rubisco performs at the maximal possible NPR for the given environment.

Discussion

Several scenarios could lead to the observed effectively one-dimensional landscape (Fig. 5B): The constraints may be strict and all feasible kinetic parameters are therefore close to the line. In another scenario, the constraints are only upper limits on the kinetic parameters and it is selection that pushes Rubisco to this limit. In both cases, the resulting observed landscape is one-dimensional, but the two scenarios differ in the accessible phenotypes. In the first, mutations cannot yield phenotypes far from the line, whereas in the latter, phenotypes far from the line are feasible but are expected to vanish rapidly by the strong selective forces. A hint that supports the latter scenario comes from the observed fluctuations of the kinetic parameters around the line. Combinations of parameters that strongly affect the NPR tend to exhibit much smaller variability. For example, the NPR does not depend directly on K_O but rather on the affinity ratio K_C/K_O (Fig. 1). Indeed, the correlation coefficient between K_O and v_C is ~ 0.5 , indicating large variability, whereas the correlation coefficient between K_C and v_C is much larger, 0.95. A possible experimental test that could map the accessible phenotypes is a statistical survey of Rubisco phenotypes (i.e., their kinetic parameters) resulting from point mutations.

The fact that the only outliers are the form II Rubisco of *R. rubrum* and *R. sphaeroides*, which lack the small subunits of form I, may indicate that the two forms of Rubisco may be subject to different constraints. Measurements of the activity of isolated large subunits, especially from the Rubisco of *Synechococcus* (32–35), indicate that the v_C is drastically reduced whereas the specificity is relatively unchanged. However, the main deviation of the form II Rubisco from the correlations is in the specificity S (Fig. 2B and C) whereas its K_C and v_C , which are the main determinants

Figure 5 consists of two panels, A and B. Panel A is a line graph showing the normalized photosynthesis rate on the y-axis (ranging from 0 to 1) against the carboxylation velocity v_C [1/sec] on the x-axis (logarithmic scale from 10^0 to 10^2). Three curves are shown for different CO_2 concentrations: $[\text{CO}_2] = 10 \mu\text{M}$ (blue), $[\text{CO}_2] = 80 \mu\text{M}$ (green), and $[\text{CO}_2] = 250 \mu\text{M}$ (red). Vertical dashed lines indicate the optimal v_C for various organisms: Nongreen algae (CCM?), C_3 plants, Nongreen algae (with CCM), C_4 plants, Green algae, Photosynthetic Bacteria, and Cyanobacteria. Panel B shows two plots of kinetic parameters. The left plot shows a shaded region of 'feasible' phenotypes (blue dots) bounded by a dashed line representing a negative correlation between two parameters. The right plot shows the same region with an arrow labeled 'selection' pointing towards the dashed line, indicating that the observed phenotypes are constrained to the edge of the feasible region.

Fig. 5. (A) Normalized NPR as a function of v_C (fully optimal Rubisco has a normalized NPR of 100%). For example, the cyanobacteria in a strong CCM environment (red line), $[\text{CO}_2] = 250 \mu\text{M}$, have normalized NPR of $\sim 99\%$. However, if one put this Rubisco in an environment typical of C_3 plants (blue line), $[\text{CO}_2] = 10 \mu\text{M}$, it would achieve only 34% of the maximal possible NPR while C_3 plants achieve normalized NPR of 95%. In accord, photosynthesis was impaired when Rubisco of *R. rubrum* replaced the native Rubisco of cyanobacteria or tobacco (30, 31). (B) The axes represent any two kinetic parameters with negative correlation (dashed line), such as S and v_C . Rubisco (blue dots) resides in an effectively one-dimensional fitness landscape (the region near the correlation line), which may be the outcome of two possible scenarios: In the first, Rubisco is confined to a limited region of phenotypes (Left). In the second, the observed relation may be only an upper limit (Right) and it is selection that pushes Rubisco to the edge.

of the NPR, obey the same power law correlations of the form I Rubisco. This may hint that this trade-off is linked to the large subunit, whereas the trade-off between $k_{\text{on,C}}$ and $k_{\text{on,O}}$ is related to the small subunit. Measurements of other form II Rubisco may further clarify the origin of this deviation.

Our analysis yields simple quantitative predictions for the response of Rubisco to changing environments (Eq. 4), which can be experimentally tested. For example, one may vary the ambient CO_2 levels or alternatively manipulate the CCM to affect the concentration at the carboxylation site. We expect that the kinetic parameters of Rubisco will adapt to the change to optimize its performance. Another possibility is to replace the Rubisco of one species by a heterologous Rubisco from a species that lives in a different environment and trace its adaptation to the environment of the host organism. We note that the NPR, f , measures the effect of Rubisco on fitness and that the overall fitness of a species should take into account resources (light, water, etc.). However, our conclusion regarding the one-dimensional landscape of Rubisco does not depend on the measure of optimality.

Our results indicate that Rubisco is close to optimality in the NPR and therefore cannot be significantly improved by point mutations. To improve the performance of Rubisco one may perhaps focus on improving the CCM rather than mutating the Rubisco itself. Nevertheless, the results do not preclude the possibility that a drastic change, such as the change between forms I and II, may result in Rubisco that is subject to different constraints, which may perhaps allow better performance.

Savir et al.

PNAS | February 23, 2010 | vol. 107 | no. 8 | 3479

Here we show that Rubisco sets an example for a protein whose plasticity is confined to a low-dimensional landscape by underlying constraints. In this confined landscape, selection forces drive it toward optimality. It demonstrates how the interplay between selection and constraints limits the plasticity of proteins and their ability to explore the phenotype space to improve their fitness. Similar trade-offs may shape the evolution of other multistage enzymes.

Methods

Effective Michaelis–Menten Parameters. The CO_2/O_2 addition to the enolized Rubisco–RuBP complex is practically irreversible, $k'_{a,C}$, $k'_{a,O} \approx 0$ (12, 36) and thus the apparent Michaelis–Menten constants for CO_2 addition (K_C) and O_2 addition (K_O) are (Fig. 1B) $K_C = (v_C/k_{a,C}) \cdot (k_e + k'_e)/k_e$ and $K_O = (v_O/k_{a,O}) \cdot (k_e + k'_e)/k_e$. There is an uncertainty as to whether the addition of gas and water is sequential or concerted (12). In the sequential case, CO_2 addition results in a six-carbon carboxyketone intermediate that is followed by a gem-diol hydrate intermediate that, in turn, undergoes cleavage. In the concerted case, there is only a hydrated intermediate, which undergoes cleavage. Experimental data suggest that the six-carbon intermediate is stabilized on enzyme mostly in its hydrate form and imply that hydration may be irreversible (37). At physiological pH values, enolization should be faster than the maximal catalytic rate, v_C , $v_O \ll k_e$ (38, 39). Thus, the maximal rates of carboxylation (v_C) and oxygenation (v_O) take the form $v_C = k_{\text{cle},C} \cdot k_{\text{H}_2\text{O}}/(k_{\text{cle},C} + k_{\text{H}_2\text{O}})$ and $v_O = k_{\text{cle},O} \cdot k_{\text{H}_2\text{O}}/(k_{\text{cle},O} + k_{\text{H}_2\text{O}})$. If the gaseous addition and hydration are concerted, then $v_C = k_{\text{cle},C}$ and $v_O = k_{\text{cle},O}$.

PCA and Total Least-Squares Analysis. The data set contains four variables that determine the NPR (K_C , v_C , S , K_C/K_O) and represent points in a 4D space. For 28 Rubiscos S and K_C are known. From these 28, for 25 Rubiscos K_O is known and from these 25, for 16 Rubiscos v_C is known. We performed PCA (40) on the data from the 16 Rubiscos for which all four kinetic parameters are available, excluding the form II *R. rubrum* outlier. The eigenvalues of the covariance matrix (the latent vector) are [3.6, 0.25, 0.09, 0.02] and their proportions are [91%, 6%, 2%, 1%]. To account for the rest of the Rubiscos, we performed a total least-squares fit on the entire set. We find the parameters that minimize the distance between the data points in logarithmic scale and the line (which represents our model) ($t, \alpha t + \beta, \alpha_1 t + \beta_1, \alpha_2 t + \beta_2$). The results yield the following power laws:

$$\begin{aligned} K_C &= 1.32 \pm 0.5 \cdot v_C^{2.03 \pm 0.2} \left([0.49 \ 2.54]; [1.68 \ 2.56] \right), \\ S &= 152 \pm 28 \cdot v_C^{-0.51 \pm 0.1} \left([111 \ 245]; [-0.76 \ -0.34] \right), \quad [5] \\ K_O &= 239 \pm 50 \cdot v_C^{0.57 \pm 0.1} \left([136 \ 347]; [0.37 \ 0.87] \right) \end{aligned}$$

The confidence bounds (95%) for the prefactor and the exponent are in brackets. In the total least-squares process, we excluded two evident outliers, the form II of *R. rubrum* and *R. sphaeroides* (*R. sphaeroides* was not part of the PCA data).

ACKNOWLEDGMENTS. We thank J. Berry, G. Farquhar, A. Kaplan, I. Matsumura, A. Bar-Even, L. Aimola, U. Alon, M. Gurevitz, Y. Marcus, E. Moses, Y. Hart, M. Holbrook, D. Bensimon, A. Libchaber, P. Gulobinoff, and A. Schertz and the support of the Minerva foundation and Israel Science Foundation.

- Ellis RJ (1979) The most abundant protein in the world. *Trends Biochem Sci* 4:241–244.
- Andrews TJ, Lorimer GH (1978) Photorespiration—Still unavoidable? *FEBS Lett* 90:1–9.
- Lorimer GH, Andrews TJ (1973) Plant photorespiration—An inevitable consequence of the existence of atmospheric oxygen. *Nature* 243:359–360.
- Andersson I, Backlund A (2008) Structure and function of Rubisco. *Plant Physiol Biochem* 46:275–291.
- Bowsher C, Steer M, Tobin A (2008) *Plant Biochemistry* (Taylor & Francis, New York).
- Christoph P, Markus N, Rashad K (2008) Metabolic engineering towards the enhancement of photosynthesis. *Photochem Photobiol* 84:1317–1323.
- Mueller-Cajar O, Whitney S (2008) Directing the evolution of Rubisco and Rubisco activase: First impressions of a new tool for photosynthesis research. *Photosynth Res* 98:667–675.
- Parikh MR, Greene DN, Woods KK, Matsumura I (2006) Directed evolution of RuBisCO hypermorphs through genetic selection in engineered *E. coli*. *Protein Eng Des Sel* 19:113–119.
- Jordan DB, Ogren WL (1981) Species variation in the specificity of ribulose biphosphate carboxylase/oxygenase. *Nature* 291:513–515.
- Tcherkez GG, Farquhar GD, Andrews TJ (2006) Despite slow catalysis and confused substrate specificity, all ribulose biphosphate carboxylases may be nearly perfectly optimized. *Proc Natl Acad Sci USA* 103:7246–7251.
- Cleland WW, Andrews TJ, Gutteridge S, Hartman FC, Lorimer GH (1998) Mechanism of Rubisco: The carbamate as general base. *Chem Rev* 98:549–562.
- Roy H, Andrews TJ (2000) In *Photosynthesis: Physiology and Metabolism*, eds Leegood RC, Sharkey TD, von Caemmerer S (Kluwer, Dordrecht, The Netherlands), pp 53–83.
- Farquhar GD (1979) Models describing the kinetics of ribulose biphosphate carboxylase-oxygenase. *Arch Biochem Biophys* 193:456–468.
- Hatch M (1992) C4 photosynthesis: an unlikely process full of surprises. *Plant Cell Physiol* 33:333–342.
- Kaplan A, Reinhold L (1999) CO_2 concentrating mechanisms in photosynthetic microorganisms. *Annu Rev Plant Physiol Mol Biol* 50:539–570.
- Badger MR, Spalding MH (2000) *Photosynthesis: Physiology and Metabolism*, eds Leegood RC, Sharkey TD, von Caemmerer S (Kluwer, Dordrecht, The Netherlands).
- Gould SJ, Lewontin RC (1979) The spandrels of San Marco and the panglossian paradigm: A critique of the adaptationist programme. *Proc R Soc Lond B* 205:581–598.
- Somerville C, Fitch J, Somerville S, McIntosh L, Nargang F (1984) *Advances in Gene Technology: Molecular Genetics of Plants and Animals*, eds Downey K, Voellmy RW, Schultz J, Ahmad F (Academic, New York), pp 295–309.
- Zhu X-G, Portis AR, Long JSP (2004) Would transformation of C_3 crop plants with foreign Rubisco increase productivity? A computational analysis extrapolating from kinetic properties to canopy photosynthesis. *Plant Cell Environ* 27:155–165.
- Jordan DB, Ogren WL (1983) Species variation in kinetic properties of ribulose 1,5-biphosphate carboxylase/oxygenase. *Arch Biochem Biophys* 227:425–433.
- Savir Y, Tlusty T (2007) Conformational proofreading: The impact of conformational changes on the specificity of molecular recognition. *PLoS One* 2:e468.
- Savir Y, Tlusty T (2008) Optimal design of a molecular recognizer: Molecular recognition as a Bayesian signal detection problem. *IEEE J Sel Topics Signal Process* 2:390–399.
- Lorimer GH, Chen YR, Hartman FC (1993) A role for the epsilon-amino group of lysine-334 of ribulose-1,5-biphosphate carboxylase in the addition of carbon dioxide to the 2,3-enediol(ate) of ribulose 1,5-biphosphate. *Biochemistry* 32:9018–9024.
- Spreitzer RJ, Salvucci ME (2002) Rubisco: Structure, regulatory interactions, and possibilities for a better enzyme. *Annu Rev Plant Biol* 53:449–475.
- Furbank RT, Hatch MD (1987) Mechanism of C_4 photosynthesis: The size and composition of the inorganic carbon pool in bundle sheath cells. *Plant Physiol* 85:958–964.
- Fridlyand LE (1997) Models of CO_2 concentrating mechanisms in microalgae taking into account cell and chloroplast structure. *Biosystems* 44:41–57.
- Hatch MD (1971) The C_4 -pathway of photosynthesis. Evidence for an intermediate pool of carbon dioxide and the identity of the donor C_4 -dicarboxylic acid. *Biochem J* 125:425–432.
- Badger MR, et al. (1998) The diversity and coevolution of Rubisco, plastids, pyrenoids, and chloroplast-based CO_2 -concentrating mechanisms in algae. *Can J Bot* 76:1052–1071.
- Fridlyand L, Kaplan A, Reinhold L (1996) Quantitative evaluation of the role of a putative CO_2 -scavenging entity in the cyanobacterial CO_2 -concentrating mechanism. *Biosystems* 37:229–238.
- Pierce J, Carlson TJ, Williams JG (1989) A cyanobacterial mutant requiring the expression of ribulose biphosphate carboxylase from a photosynthetic anaerobe. *Proc Natl Acad Sci USA* 86:5753–5757.
- Whitney SM, Andrews TJ (2003) Photosynthesis and growth of tobacco with a substituted bacterial Rubisco mirror the properties of the introduced enzyme. *Plant Physiol* 133:287–294.
- Andrews TJ (1988) Catalysis by cyanobacterial ribulose-biphosphate carboxylase large subunits in the complete absence of small subunits. *J Biol Chem* 263:12213–12219.
- Gutteridge S (1991) The relative catalytic specificities of the large subunit core of *Synechococcus* ribulose biphosphate carboxylase/oxygenase. *J Biol Chem* 266:7359–7362.
- Lee BG, Read BA, Tabita FR (1991) Catalytic properties of recombinant octameric, hexadecameric, and heterologous cyanobacterial/bacterial ribulose-1,5-biphosphate carboxylase/oxygenase. *Arch Biochem Biophys* 291:263–269.
- Morell MK, Wilkin JM, Kane HJ, Andrews TJ (1997) Side reactions catalyzed by ribulose-biphosphate carboxylase in the presence and absence of small subunits. *J Biol Chem* 272:5445–5451.
- Pierce J, Andrews TJ, Lorimer GH (1986) Reaction intermediate partitioning by ribulose-biphosphate carboxylases with differing substrate specificities. *J Biol Chem* 261:10248–10256.
- Lorimer GH, Andrews TJ, Pierce J, Schloss JV (1986) 2'-Carboxy-3-keto-D-arabinitol 1,5-biphosphate, the six-carbon intermediate of the ribulose biphosphate carboxylase reaction. *Philos Trans R Soc B* 313:397–407.
- Pierce J, Lorimer GH, Reddy GS (1986) Kinetic mechanism of ribulosebiphosphate carboxylase: Evidence for an ordered, sequential reaction. *Biochemistry* 25:1636–1644.
- Saver BG, Knowles JR (1982) Ribulose-1,5-biphosphate carboxylase: Enzyme-catalyzed appearance of solvent tritium at carbon 3 of ribulose 1,5-biphosphate reisolated after partial reaction. *Biochemistry* 21:5398–5403.
- Shaw PJA (2003) *Multivariate Statistics for the Environmental Sciences* (Hodder-Arnold, London).